Congress on Numerical Methods in Engineering 2011
Coimbra, 14 to 17 June, 2011

NUMERICAL SIMULATION OF THE STRUCTURAL BEHAVIOUR OF CONCRETE TETRAPODS SUBJECT TO IMPOSED DEFORMATIONS AND APPLIED LOADS

Miguel Azenha[1]*, José Sena Cruz[1], Aires Camões[2] and Rui Miguel Ferreira[2]

1: ISISE – Institute for Sustainability and Innovation in Structural Engineering
Departamento de Engenharia Civil - Escola de Engenharia
Universidade do Minho
4800-058 Guimarães
e-mail: {miguel.azenha,jsena}@civil.uminho.pt, web: http://www.isise.net

2: C-TAC – Centro de Território, Ambiente e Construção
Departamento de Engenharia Civil - Escola de Engenharia
Universidade do Minho
4800-058 Guimarães
e-mail: {aires,rmf}@civil.uminho.pt, web: http://www.civil.uminho.pt/c-tac

Keywords: Tetrapod, concrete, heat of hydration, internal reinforcement

Abstract *Tetrapods for coastal protection are frequently used in break waters for dissipation of wave energy. During their service, these plain concrete elements usually exhibit degradation signs with frequent premature rupture of one or more of their legs when located in highly aggressive environments subjected to extreme wave action. These ruptures tend to decrease the efficiency of breakwaters as a whole, thus diminishing their capacity to absorb wave energy. The present paper aims to contribute to a better understanding of the stress levels that occur in this kind of mass concrete elements, taking into account imposed deformations (associated with heat of hydration) and applied loads. A thermo-mechanical numerical simulation tool (3D), based on the finite element method, is used for the assessment of heat of hydration induced stresses. After an initial discussion of the temperature development inside the tetrapod, the corresponding residual stresses are presented and discussed, and conclusions are withdrawn with regard to the available capacity of concrete to withstand further applied loads. Finally, the subsequent behaviour of the tetrapod is assessed and compared to alternative solutions with internal reinforcement of the tetrapod legs, such as reinforced concrete (using stainless steel), steel fibre reinforced concrete and reinforced concrete with FRP's.*

1. INTRODUCTION

The use of tetrapods for breakwaters construction has been generalized throughout the world for decades. Tetrapods are usually made of plain concrete, having four legs that irradiate from a central point, with leg diameters that can increase up to 2m and total tetrapod height over 4m. During their service life, tetrapods are known to frequently suffer severe degradation (mainly cracking) and subsequently premature rupture of its legs. The collapse of tetrapods contributes to a decrease in the efficiency of the breakwater system as a whole, and thus leads to a reduced capacity for energy absorption. It is therefore essential to ensure the maintenance of the geometry of the tetrapods for the longest time possible. In fact, in order to maintain adequate levels of hydraulic performance of the breakwater, the removal of loose ends of fractured tetrapods, as well as the substitution of the damaged tetrapods is a necessity and results in significant maintenance costs that justify the study of solutions that minimize the need for this kind of intervention.

The owner of a breakwater located in the North of Portugal has recently reported the occurrence of several ruptures in tetrapods under service conditions, and requested evaluation of possible ways to overcome this problem. The present paper regards to a part of the developed work performed at the University of Minho, with regards to: (i) the assessment of the thermal stresses generated at early ages and their potential to create fragilities in the tetrapods; (ii) evaluation of alternate ways of internally reinforcing the tetrapod so that its load capacity can be increased.

To pursue the objective (i) mentioned above, a 3D thermo-mechanical analysis based on the finite element method is presented in Section 2, with specific details on the modelling approach and detailed discussion of computed temperatures and stresses.

The analysis of alternative solutions for internal reinforcement of the tetrapod is discussed in Section 3, where the study of the following solutions is reported: reinforced concrete (using stainless steel), steel fibre reinforced concrete and reinforced concrete with FRP's.

2. THERMO-MECHANICAL ANALYSIS

2.1. General remarks

The present section regards to the thermo-mechanical modelling of the tetrapod with the finite element method, and a brief description of the modelling options. Specific details about the governing equations and background information on the implementation can be found in [1]. It is intended to find out whether the self-induced stresses associated to heat of hydration release (and consequent temperature variations) are relevant enough to be considered partially responsible for the insufficient service-life behaviour usually observed in this kind of element.

The analysed tetrapod is made of plain concrete, with the composition shown in Table 1:

	Quantity (kg/m^3)
CEM I 42.5R	205
Fly ash	105
Sand	590
Course aggregate (4-65mm)	1360
Water	140
Superplasticizer	3.1

Table 1. Mix proportions of the concrete mix (C25/30)

2.2. Geometry and finite element mesh

The tetrapod under study and used in the breakwater in question is a SOTRAMER 40t [2], which dimensions are depicted in Figure 1. Most of the features of this geometry have been contemplated in the finite element (FE) mesh shown in Figure 2, where solid pyramid finite elements where used. Both thermal and mechanical analyses were conducted with this FE mesh, but with different number of nodes per element: (i) in the thermal analysis, 4 node elements where adopted, whereas; (ii) for the mechanical analysis, each pyramid element had 10 nodes. All outer boundaries of the tetrapod have 3 node surface elements, adopted in the scope of the thermal analysis to account for convection/radiation boundary conditions. The final mesh has a total of 22556 nodes and 17771 elements.

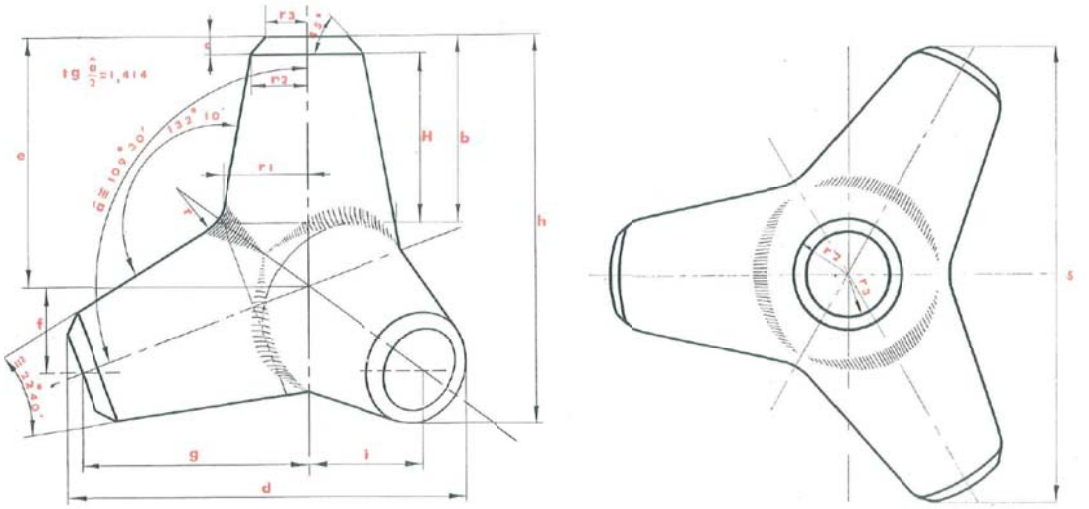

Mass (ton)	h	d	s	r.1	r.2	r.3	H	b	c	r_{recom}	r_{min}	e	f	g	i
								(mm)							
40	3860	4025	4620	920	575	420	1715	1870	155	645	355	2520	840	2380	1190

Figure 1. Geometrical information of SOTRAMER 40t tetrapod.

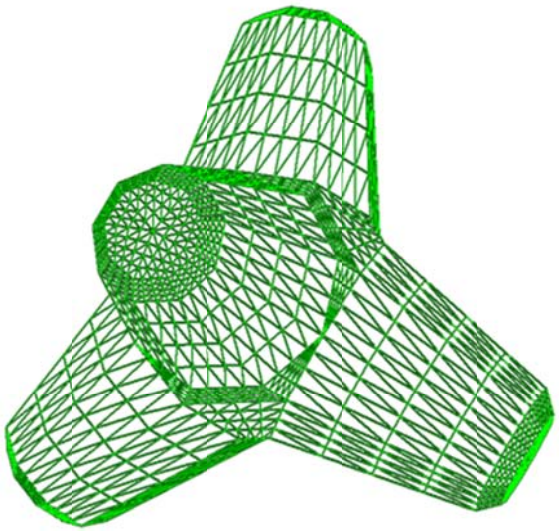

Figure 2. 3D finite element mesh adopted for the tetrapod.

2.3. Thermal properties and boundary conditions

Regarding the thermal conductivity (k) and specific heat of concrete (ρc), the following reference values have been adopted: k = 2.6 $Wm^{-1}K^{-1}$ and ρc = 2400 $kJm^{-3}K^{-1}$. The previous experience of the team in the use of these reference parameters, with success in the prediction of temperature fields in concrete since early ages, led to the choice of not determining these values experimentally in the scope of this work [1].
The heat generation of concrete was modeled with recourse to a formulation based on the Arrhenius law, and the experimental data reported in [1] for the type of cement (and brand) used for the tetrapod: CEM I 42.5R (Company A, as mentioned in reference [1]). The heat generation has been dully adapted to the volumetric content of cement in the mix. Instead of using the cement content of 205 kgm^{-3} (according to Table 1), it was decided to study an extreme scenario of replacing the total binder content (cement + fly ash) with only cement, resulting in a total cement content of 310 kgm^{-3}.

The actual thermal boundary conditions of the tetrapod are not constant in time neither along the tetrapod. In fact, the bottom surfaces of the tetrapod are initially supported by a concrete base, and the lateral surfaces correspond to formwork, which is eventually removed. However, due to the complexities of the model geometry, it was decided to make some simplifications to the boundary conditions. Therefore, all surfaces of the tetrapod were considered to have the same thermal boundary condition along time, in correspondence to direct contact with the surrounding environment (with a convection/radiation coefficient of 10 $Wm^{-2}K^{-1}$ related to wind speeds lower than 10km/h). Furthermore, in order to simplify the interpretation of results, the environmental temperature was considered constant with value T=20ºC. These deviations of boundary conditions and environmental temperature in regard to actual in-situ situations are

considered to have relatively low impact in the accuracy of calculated temperatures, as the high volume of the tetrapod, combined with the high thermal inertia of concrete, diminish the sensitivity of results to the boundary conditions. Therefore, it is considered that the ease of modelling and interpretation associated to this set of simplifications represent a significant enough advantage in regard to the actual drawback of potential inaccuracies in the computed temperatures.
The initial temperature of concrete was considered to be coincident with that of the environment: T=20ºC.

2.4. Mechanical properties and boundary conditions

As the conducted study aims to evaluate cracking risk associated to early temperature variations (heat of hydration), without specific focus on the post-cracking behaviour, the mechanical analyses neglect the possibility of cracking. This modelling option will be checked later in this paper upon analysis of the results of the mechanical analysis.
In view of the purpose to evaluate early stresses induced by the non-uniform temperature field that occurs in concrete due to heat of hydration development, two of the main issues to bear in mind for the mechanical analyses are: the evolution of concrete E-modulus since its early ages; the viscoelastic behaviour of concrete (creep). As the characterization of these mechanical properties was not possible, it was decided to use values from mechanical characterizations recently carried out at the University of Minho, obtained for a concrete with similar strength as that used for the tetrapods [3]. Also, for the E-modulus of concrete, results gathered using the recently proposed methodology by Azenha et al. [4] were used, providing quantitative information about the structural setting time, as well as the detail evolution of E-modulus along early ages, as shown in Figure 3.

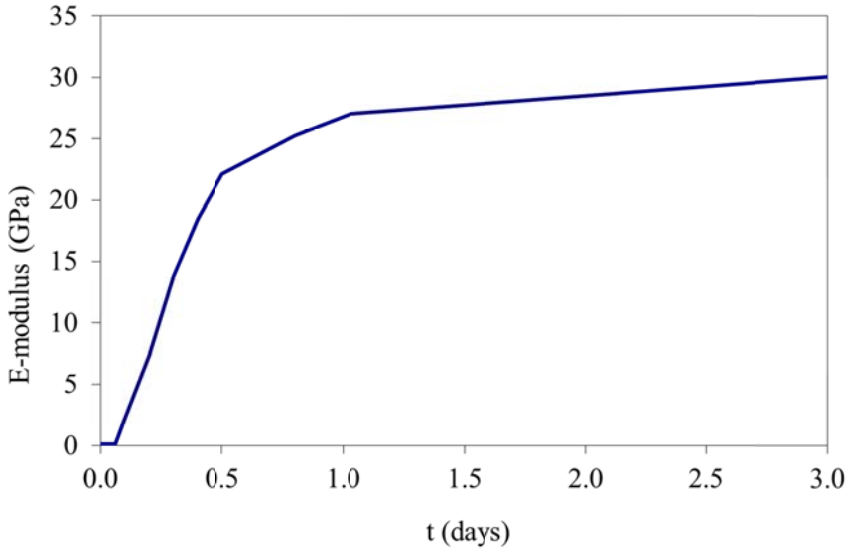

Figure 3. Evolution of concrete E-modulus along the initial 3 days.

The value of 0.2 was adopted for Poisson's coefficient, neglecting its variation at early ages, which has been shown to have negligible influence in thermal stress development according to [1]. The thermal dilation coefficient was also considered constant throughout the analysis with the value $10\times10^{-6}K^{-1}$. In order to simulate the creep behaviour of concrete, the Double Power Law [5] was used with the following parameters (unit of time: days): $\phi = 0,8$; $m = 0,2$; $n = 0,3$.

As drying shrinkage assumes negligible values at early ages (small drying time) and at later ages (as this is a structural element that is frequently being partially submerged), and bearing in mind the low expectable values for autogenous shrinkage (due to the relatively low cement content), it was decided to disregard the effect of shrinkage in the analyses of this research.

As far as mechanical boundary conditions are concerned, three point supports were considered in the three legs of the tetrapod that contact with the ground. These point supports restrain vertical displacements, but allow the tetrapod to expand or contract freely with regards to a horizontal plane: these support conditions intend to simulate the placement of the tetrapod over a horizontal surface. This corresponds to a simplification of the actual support conditions right after casting, as the tetrapod is supported in all the lower surface of three legs (as mentioned above). However, it is considered that this support simplification does not affect the accuracy of computed stresses, as the main stresses are caused by expansion/contraction of the tetrapod which is not actually hindered by the supports. It should also be remarked that the self-weight of the tetrapod is being neglected in the analyses, as it causes negligible stress levels in concrete.

Both thermal and mechanical simulations were conducted for a total period of analysis of 6 days, divided in 1-hour long steps (total of 144 steps).

2.5. Results of the thermal model

For illustration of the temperature fields calculated for a set of relevant instants, the tetrapod is represented by its cross-section through a vertical plane that intersects the longitudinal axis of one of the lower legs. The corresponding temperature maps for instants t=10h, t=20h, t=30h, t=36h, t=50h, t=80h, t=120h and t=144h are shown in Figure 4.

Before starting to discuss the temperatures that have just been depicted, additional information is given in the form of a XY graphic with the plot of calculated temperatures throughout the analysis for both the geometrical centre of the tetrapod and a surface point (located at mid-height of the vertical leg) – see Figure 5.

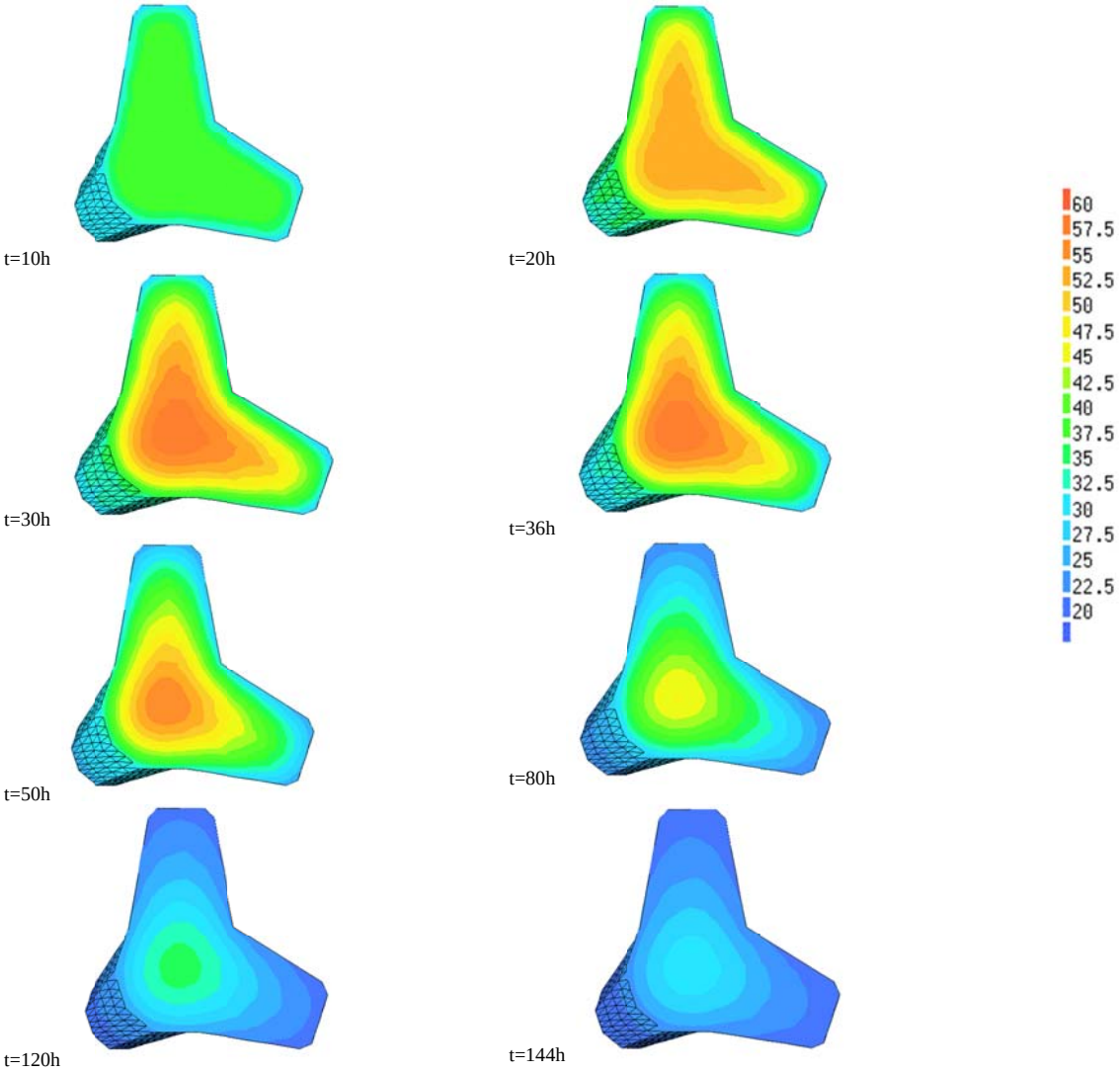

Figure 4. Temperature distribution in the tetrapod for a set of relevant instants (T in ºC)

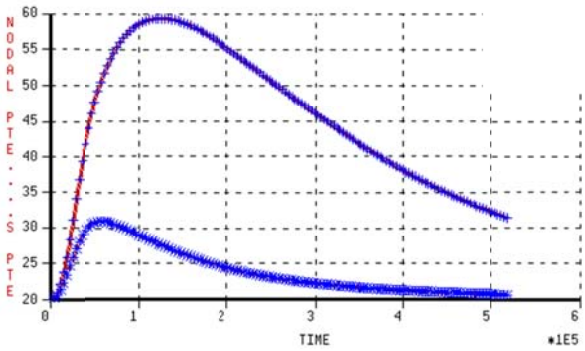

Figure 5. Temperature evolution for the geometrical centre of the tetrapod (higher temperatures) and for a point located in the surface at mid-height of the vertical leg – time in seconds and temperature in ºC

Based on the set of figures related to temperature development that have been shown, the following observations can be made:

- As expectable, the highest temperatures are attained in the geometrical centre of the tetrapod, whereas the lowest temperatures occur near the surfaces;
- The maximum calculated temperature is approximately 59ºC, occurring at t=36h, in the geometric centre of the tetrapod;
- The maximum thermal gradient also occurs at t=36h, with approximately 30ºC of difference between surface temperatures and interior temperature;
- The duration of analysis of 144 hours was not enough to allow the entire volume of the tetrapod to attain thermal equilibrium with the surrounding environment (i.e. uniform temperature T=20ºC). However, given the monotonic tendency of temperature decrease in the tetrapod, it would be expectable to attain such equilibrium within an additional period of 24 to 48 hours (see Figure 5). It was not considered necessary to conduct a new analysis for a longer time due to the fact that its results are easily inferred;
- Even though the geometrical centre of the tetrapod is not at thermal equilibrium with the environment at the end of the analysis (t=144h), Figure 4 allows observing that at this instant, most of the tetrapod's legs has cooled to approximately 20ºC.

2.6. Results of the mechanical model

The evolution of the maximum principal stress in the point located at the geometric centre of the tetrapod (in which the maximum temperature change has been reported) is plotted in Figure 6. Through interpretation of this Figure, it is observed that during the heating phase, concrete becomes compressed until a maximum of 1.3 MPa (the state of compression is understandable, as the core heats more than surface areas, so, the resulting differential expansion ends up causing tensile stresses in the surfaces and compressive stresses in the core). The cooling phase leads to the progressive diminishment of

compressive stresses until the core starts enduring tensile stresses. The maximum principal stress in the geometrical centre of the tetrapod at the end of the analysis amounts to approximately 0.4MPa, with a slight increasing tendency until attainment of thermal equilibrium with the surrounding environment. If the numerical analysis had been extended for a larger period of time, slightly larger tensile stresses would have been computed. Bearing in mind the expectable tensile strength for the concrete used (around 2 MPa, or larger) it becomes clear that thermal cracking is not expectable in the interior areas of the tetrapod.

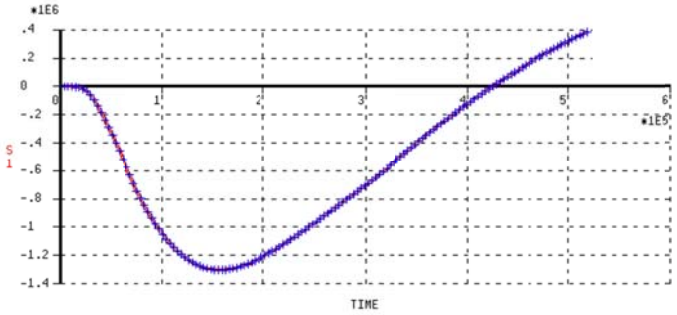

Figure 6. Maximum principal stress in the point located at the geometric centre of the tetrapod – time in seconds and stress in Pa

Higher cracking risks are observed (both in heating and cooling phases) in the legs of the tetrapod. To illustrate this statement, a horizontal cross-section of the vertical tetrapod leg, at the height of 2.2m from the horizontal supporting surface, is analysed for its maximum principal stresses. These stresses are represented in Figure 7 for the instants t=18h (instant of maximum cracking risk for the surface areas) and t=144h (instant where maximum cracking risk is observable in the core of the leg). It is seen that at t=18h (heating phase), the maximum tensile stresses occur at the surfaces, with values of circa 1MPa. The cracking risk for surface areas at this instant cannot be considered negligible, as this is an instant at which the tensile strength of concrete is still evolving, and may still have values that are bellow or similar to the calculated acting stress.

At the end of the cooling stage, particularly for the instant t=144h, shown in Figure 7, it is observed that the maximum tensile stresses are located in the centre of the tetrapod's leg, with value under 1MPa. In this case, the cracking risk of the tetrapod's leg is clearly lower than that of the surface areas, because the tensile stress is lower, and also because this is an instant at which the tensile strength of concrete is much higher than at t=18h.

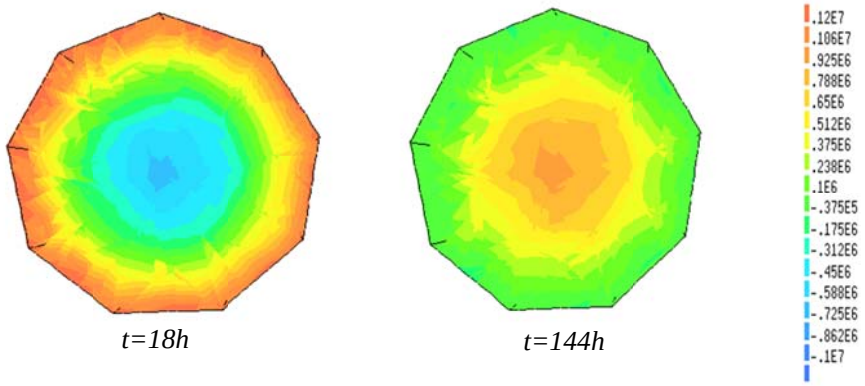

Figure 7. Maximum principal stresses in the tetrapod for a cross-section of the vertical leg at an height of 2.2m: a) at t= 18h; b) at t=144h - stress in Pa

Finally, a map representation of the principal stresses at the surface of the tetrapod is presented for the instant of maximum surface cracking risk (t=18h) in Figure 8. The maximum stress shown in Figure 7 for the surface region of the tetrapod's leg is now confirmed for most of the tetrapod's surface, putting into evidence the non-negligible risk of cracking for these areas during the heating phase.

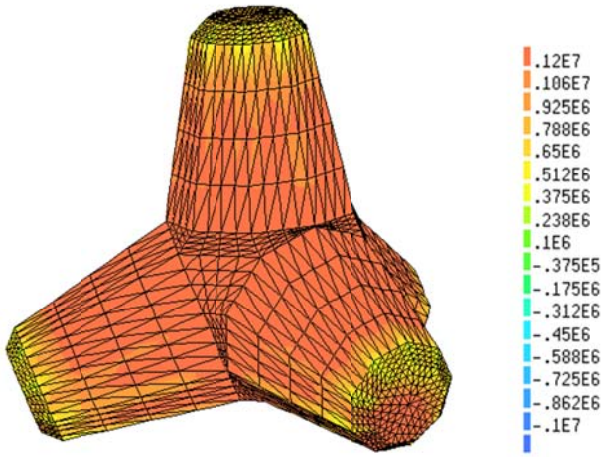

Figure 8. Map representation of the principal stress on the tetrapod at t=18h - stress in Pa

With basis on the gathered results, it is possible to infer that:

- Even though large temperature gradients were observed, the absence of external restraint to deformation led the internal stresses to be caused solely by temperature differences between different zones of the tetrapod. As the self-restraint effect to thermal deformations was relatively small, the resulting

tensile stresses ended up having low significance;

- The risk of surface cracking is relevant during the heating phase (until t=36h), whereas since then, the tensile surface stresses start diminishing and even revert their sign, becoming compressive. Even if surface cracking (or micro-cracking) occurs during the heating phase, the cracks should exhibit a tendency to close and remain compressed after the whole tetrapod has cooled;
- In the core areas of the tetrapod (both in its geometrical centre, and in the interior zones of the legs), tensile stresses are observed during the cooling phase, with a lower cracking risk than the one that had been identified for surface areas (bearing in mind that the tensile strength of concrete is higher during the cooling phase than during the heating phase);
- Based on the obtained results, even though there is a non-negligible thermal cracking risk of the surface zones of the tetrapod (during the heating phase), it is considered that the potential associated cracking could not cause enough damage to the tetrapod as to justify many of the ruptures observed in service conditions for these elements. Furthermore, it is considered that the sensitivity analyses to be presented in Section 4, which focus in alternative solutions for internal reinforcement of the tetrapod, may disregard internal stresses associated to heat of hydration without affecting the conclusions that can be withdrawn for ultimate limit state capacity of the tetrapod;
- The simplifications adopted in the calculations naturally cause deviations between calculated temperatures and stresses, in regard to what actually happens for in-situ construction. Nonetheless, based on the accumulated experience gathered by the authors, as well as on a set of parametric analyses reported in [1], it is considered that the plausibility of the results is not jeopardized. It is thus considered that the conclusions which would be obtained upon a detailed material characterization and a more realistic modelling of boundary conditions, would be quite similar to those presented in this research;
- A final remark is given with regards to the added value obtained by performing a 3D analysis of the tetrapod. In fact, no previous works were found to focus on this kind of approach for thermo-mechanical modelling of tetrapods, with most works focusing on simplified axisymmetric modelling of one of the legs of the tetrapod [6, 7], with special care taken in regard to thermal and mechanical boundary conditions. Within the scope of the present research, the 2D analysis was also conducted for the same tetrapod (not included in this paper for the sake of brevity), leading to a remarkably similar result in terms of calculated temperatures. However, the computed stresses with the 2D analysis tend to be clearly higher, indicating that the simplified mechanical boundary conditions assumed in the 2D modelling cause an overestimation of the restraint to deformation of the tetrapod.

3. ALTERNATIVES FOR REINFORCEMENT OF THE TETRAPODS

3.1. General remarks

There are several ways of reinforcing/strengthening plain concrete structures, mainly by the use of internal reinforcements, prestressing, jacketing or by the use of cementicious composites with high post-cracking tensile strength. In terms of the internal reinforcements, stainless steel or Fibre Reinforced Polymer (FRP's) are the more suitable materials, due the severe exposure conditions of the tetrapods. However, in spite of its the excellent corrosion resistance, solid stainless steel reinforcing rebar can sustain pitting corrosion and therefore the effectiveness of its use raises some doubts. On the other side, FRP's are identified as corrosion resistant materials [8]. In general, prestressing yields to excellent serviceability behaviour. However, the use of this technique for the present structural system is not recommended due to technical limitations and levels of prestress required. Jacketing can be applied by the use of either reinforced concrete layers or steel plates or FRP sheets. In the present analysis this retrofitting technique was not considered due to tremendous difficulties in applying the reinforcing materials to such complex geometry. Finally, the fiber reinforced concrete (FRC) can be suitable in this type of structures, since ductility, high post-cracking tensile strength, high compressive stiffness and strength can be achieved.
The quantification of the actions acting on the tetrapods is quite complex. In addition, according to the search performed by the authors of the present work, no specific standard was found for defining the actions on this type of structures. For these reasons the numerical analysis presented herein is based on a cross-sectional study of different alternatives for reinforcement of the tetrapods.

3.3. Numerical modelling

With the aim of evaluating the efficiency of different reinforcing techniques in order to increase the load carrying capacity of tetrapods, a numerical study was carried out. For this purpose each leg of the tetrapods was assumed as a cantilever beam. The fixed end section was analysed with DOCROS section-sectional layer model [9].
The numerical tool DOCROS has been developed at the University of Minho. Based on Bernoulli theory this software analyses cross-sections and the following assumptions are taken into account: (i) the plane section remains plane after deformation; and, (ii) perfect bond between materials (e.g. steel and concrete) is assumed. The section is divided in layers parallel to the direction of bending moment axis. Each thickness and width layer is user-defined and depends on the geometrical cross-section. DOCROS can analyze sections of irregular shape and size, composed of different material type, submitted to an axial force and a curvature increment following the x-axis. Each layer can have an initial non-null stress. The software can also analyze sections by phases as can be the case of retrofitting and strengthening, where additional material is active in later phases. A wide library of material constitutive laws is available for the simulation of distinct materials [9].

In the present study the following scenarios were analysed:

i) Plain concrete (PC) – reference case;
ii) Reinforced concrete with stainless steel rebars (RC-STEEL);
iii) Reinforced concrete with carbon fibre reinforced polymer (CFRP) rods (RC-CFRP);
iv) Steel fibre reinforced concrete (RC-SF);
v) Steel fibre and reinforced concrete (RC-SF+STEEL).

Thus, the cross section of the fixed end section of a leg of the tetrapod, with a diameter of 1840 mm was discretized by 20 layers with constant thickness.

For the simulation of plain concrete under compression the uniaxial constitutive law proposed by CEB-FIP Model Code 1990 [10] was adopted. For the case of PC, RC-STEEL and RC-CFRP the tensile pre- and post-peak behaviour of the concrete was also modelled with the proposal of CEB-FIP Model Code 1990 [10]. The following mechanical properties of concrete (grade C25/30) were assumed:

- Average compressive strength of concrete, f_{cm} = 33 MPa;
- Initial modulus of elasticity of concrete, E_{cm} = 31 GPa;
- Average value of tensile strength of concrete, f_{ctm} = 2.6 MPa;
- Fracture energy, G_f = 0.1338 N/mm.

The simulation of stainless rebars followed the constitutive laws proposed by the standard NP EP 1992-1-1:2010 [11], with the following mechanical properties:

- Yielding tensile stress of steel, f_y = 500 MPa;
- Modulus of elasticity of steel, E_s = 200 GPa.

Three distinct cases were analysed in terms of number of stainless rebars: 36ϕ16, 36ϕ20 and 36ϕ25. The first case corresponds to the minimum amount of reinforcement to control cracking in areas where tension is expected. The two other cases were considered with higher amounts of reinforcement.

Two hypotheses were studied for the case of the tetrapods reinforced with CFRP rods: 36 and 72 rods of CFRP with 13 mm of diameter. Linear-elastic behaviour up to the failure was assumed for the CFRP with a modulus of elasticity equal to 124 GPa and a tensile strength of 1724 MPa [12].

For the cases of RC-STEEL, RC-CFRP and RC-SF+STEEL a concrete cover of 70 mm was assumed.

In the simulation of the RC-SF and RC-SF+STEEL cases, the steel fiber reinforced concrete (SFRC) under compression was assumed to be equal to that of plain concrete, i.e. using the uniaxial law proposed by the CEB-FIP Model Code 1990 [10]. However, for the case of the SFRC material under tension, a *strain hardening* behavior was assumed [13]. The simulation of this behavior was materialized by a bi-linear law, where the first branch corresponds to the linear elastic branch followed by a horizontal top branch with a tensile strength equal to 2.6 MPa.

3.3. Results

Figure 9 shows the relationship in terms of bending moment *versus* curvature for the case of plain concrete (PC) and reinforced concrete with stainless rebars (RC-STEEL). From this figure it can be concluded that the solution 36ϕ16 corresponds to the minimum amount of reinforcement to transfer the tensile stresses from concrete to the reinforcement. For the case of 36ϕ25 the ultimate resistance is 2.8 higher.

Figure 10 depicts the response obtained by the use of CFRP rods (RC-CFRP). When compared with the RC-STEEL cases, the present ones yield to higher deformations due to the low value of the modulus of elasticity of the CFRP. When 36ϕ13 and 72ϕ13 of CFRP are used, a flexural strength of 6881 kN·m and 9244 kN·m are obtained, respectively. Despite of the RC-CFRP solutions yielded to higher carrying capacity, a significant loss of ductility can be observed, when compared with the RC-STEEL cases.

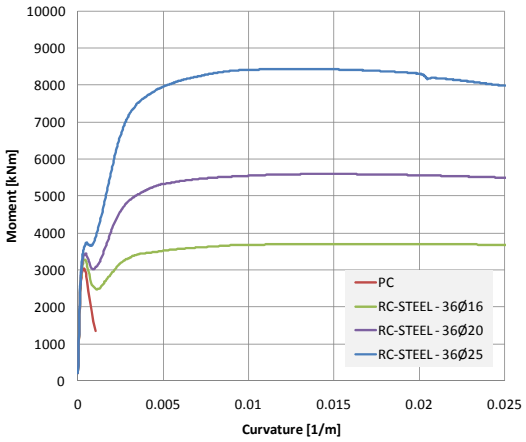

Figure 9. Moment vs. curvature for PC and RC-STEEL cases.

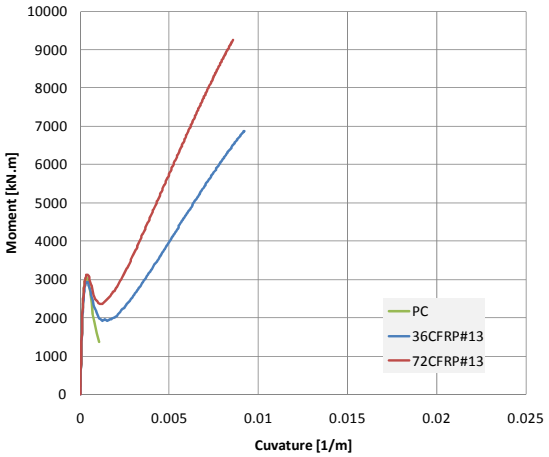

Figure 10. Moment vs. curvature for PC and RC-CFRP cases.

The analysis of the steel fibre reinforced concrete is presented in Figure 11. In this case the post-cracking behaviour is significantly changed by the addition of the steel fibres, where an increase of 1.7 was obtained when compared with the PC solution.

Finally, the last case analyzed is shown in Figure 12. In this case the response in terms of moment *versus* curvature for PC and RC-SF and RC-STEEL cases is studied. The simultaneous addition of steel fibres and stainless rebars increases in ultimate load at a factor of about 4.1.

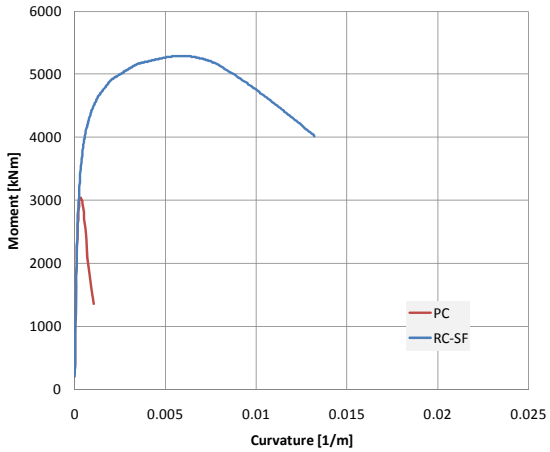

Figure 11. Moment vs. curvature for PC and RC-SF cases.

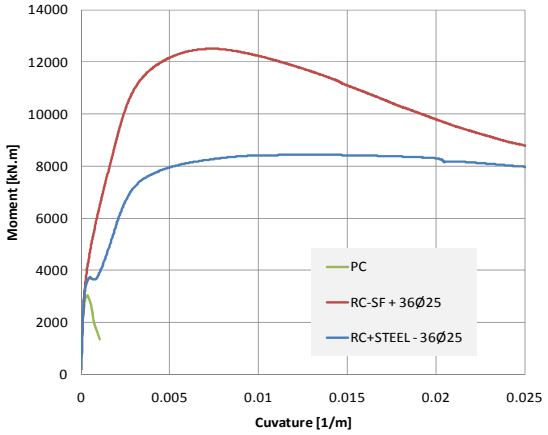

Figure 12. Moment vs. curvature for PC and RC-SF and RC-STEEL cases.

Table 2 summarizes the main results obtained in terms of load carrying capacity (M_{max}) of each solution and the ratio M_{max}/M_{ref}, where M_{ref} is equal to M_{max} obtained with plain concrete case. This table shows, from the analyzed cases, that the most efficient one is the case when the steel fibers and stainless rods are simultaneously used.

Solution	$M_{máx}$ (kN)	$M_{máx}/M_{ref}$
PC	3039.9	1.0
RC-STEEL – 36ϕ16	3701.2	1.2
RC-STEEL – 36ϕ20	5590.0	1.8
RC-STEEL – 36ϕ25	8433.1	2.8
RC-CFRP – 36ϕ13	6881.0	2.3
RC-CFRP – 72ϕ13	9244.0	3.0
RC-SF	5294.2	1.7
RC-SF+STEEL	12501.5	4.1

Table 2. Main results obtained for the load carrying capacity of the tetrapod's leg.

4. CONCLUSIONS

This paper initially comprised an in-depth analysis of the heat of hydration induced stresses that occur in a 40t SOTRAMER concrete tetrapod, leading to the conclusion that the cracking risk of this element is mainly relevant at the surface regions, during the heating stage of concrete. The cracking risk of core areas of the tetrapod is considered quite small. In the worst case scenario, some surface cracking of the tetrapod is expected during early ages, but with small depths. Even if this cracking occurs, it should tend to close during the cooling stage of concrete (with possible self-healing of the crack), so, this cracking cannot expectably be held responsible for damaging the tetrapods to an extent that justify the premature ruptures that are frequently observed in breakwaters. It is further considered that the sensitivity analyses for alternative internal reinforcement solutions for the tetrapod need not consider these internal stresses associated to heat of hydration,

without limiting the applicability of the analyses.
Distinct reinforcing techniques were analysed in order to increase the carrying capacity of the plain concrete tetrapods, mainly by the use of reinforced concrete with stainless rebars (RC-STEEL), reinforced concrete with CFRP rods (RC-CFRP), steel fibre reinforced concrete (RC-SF) and steel fibre and reinforced concrete (RC-SF+STEEL). In general, all the techniques yielded to a significant increment in terms of the ultimate load, being the RC-CFRP and RC-SF+STEEL solutions with superior performance, not only in terms of strength but also in terms of ductility.

REFERENCES

[1] Azenha, M. Numerical simulation of the structural behaviour of concrete since its early ages., PhD Thesis. Faculty of Engineering of the University of Porto, 2009.
[2] SOTRAMER. Tetrapods. Technical note., Grenoble, France, 1978.
[3] Sena Cruz, J., Barros, J., Azenha, M., Miranda, T., Carlos, K. and Silva, L. Study of cracking ocurred in the Channel Alvito/Pisão – Final report (in Portuguese). 2009.
[4] Azenha, M., Magalhães, F., Faria, R. and Cunha, A. Measurement of concrete E-modulus evolution since casting: A novel method based on ambient vibration (submitted). Cement and Concrete Research 40:1096-1105 2010.
[5] Bazant, Z. and Osman, E. Double power law for basic creep of concrete. Materials and Structures, Research and Testing, 1976;9 (49): 3-11.
[6] de Borst, R. and van den Boogaard, A. Finite-element modeling of deformation and cracking in early-age concrete. J. Engineering Mechanics Div., ASCE, 1994;120 (12): 2519-2534.
[7] Azenha, M. Behaviour of concrete at early ages. Phenomenology and thermo-mechanical analysis. (in Portuguese). MSc Thesis, Faculty of Engineering of the Univeristy of Porto, 2004.
[8] Bakis, C., LC, B., Brown, V., Cosenza, E., Davalos, J., Lesko, J., Machida, A., Rizkalla, S. and Triantafillou, T. Fiber-Reinforced Polymer Composites for Construction—State-of-the-Art Review. Journal of Composites for Construction, 2002;6 (2): 73-87.
[9] Barros, J. and Fortes, A. S. Flexural strengthening of concrete beams with CFRP laminates bonded into slits," Cement and Concrete Composites, 2005;27 (4): 471-480.
[10] CEB-FIP. Model Code 90, 1993.
[11] CEN. EN 1992-1 European Standard Eurocode 2: Design of concrete structures - Part 1: general rules and rules for buildings, 2010.
[12] AslanFRP. http://www.aslanfrp.com/Aslan200/Aslan200_CFRP_bar.html consulted in May 2011.
[13] Naaman, A. and Shah, S. P. Fracture and Multiple Cracking of Cementitious Composites. Fracture Mechanics Applied to Brittle Materials - ASTM STP 678, Part II, 1978;183-201.